Journal of the European Ceramic Society 16 (1996) 1009–1020

S0955-2219(96)00020-9
0955-2219/96/$15.00

High-temperature Fatigue of a Gas-Pressure-Sintered Silicon Nitride

M. Wang, M. Li, A. J. Bushby, F. Guiu, M. J. Reece* & M. F. R. Sammur†

Department of Materials, Queen Mary & Westfield College, Mile End Road, London E1 4NS, UK

(Received 20 September 1995; revised version received 20 December 1995; accepted 3 January 1996)

Abstract

The fatigue behaviour of a gas-pressure-sintered silicon nitride has been investigated at 1000°C. The growth of long (>100 μm) subcritical fatigue cracks was observed directly and the time to failure of uniaxially loaded specimens caused by the growth small (<100 μm), machining flaws was measured. Oxidation in the crack-tip region reduced the fatigue resistance of the material. Cracks grew under the co-operative effect of stress, oxidation and flow of the viscous oxide phase formed. This mechanism would explain why crack growth rates were greater under static loading than cyclic loading because of the more damaging effect of sustained crack opening. Because of the relatively small size of the oxidized crack-tip region and its slow advancement, the high temperature fast fracture behaviour was similar to that at room temperature and a similar value of K_{IC} *was estimated. © 1996 Elsevier Science Limited.*

1 Introduction

In recent years silicon nitride has emerged as an important ceramic for high-temperature structural applications mainly owing to its high strength, good oxidation resistance and excellent thermal shock resistance. Extensive research has been conducted on the room-temperature mechanical properties of this material and its associated composites.[1,2] It is generally recognized that the optimum microstructure of monolithic silicon nitride should consist of randomly oriented, acicular β-Si_3N_4 grains in order to achieve high strength together with high fracture toughness. Such a microstructure can provide the grain bridging and/or crack deflection mechanisms which are necessary for crack shielding and hence improve fracture toughness and flaw tolerance. However, the amount and composition of residual glass after sintering as a result of using oxide additives such as MgO, Al_2O_3 and/or Y_2O_3 to assist the α-Si_3N_4 to β-Si_3N_4 transformation and densification, affect the high temperature properties, particularly creep, of the ceramic.

If silicon nitride components are to be subjected to high-temperature exposure as well as sustained cyclic loading in service, the accumulation of damage in the material due to oxidation and stress loading needs to be understood and predictable before ceramic components can be used confidently.[3] However, only limited work has been done and we are still a long way from being able to predict accurately the long-term performance of silicon nitride components.

The mechanical fatigue behaviour of ceramic materials has attracted increasing attention ever since it was found that ceramics are, like metals, susceptible to a degradation of properties when subjected to fluctuating loading.[4] More recent experimental results show that subcritical crack growth can occur in various ceramics and ceramic matrix composites during static and cyclic loading at room temperature.[5–13] Generally, cyclic loading is more detrimental than static loading at room temperature, with higher crack growth rates under cyclic loading than under static loading at the same maximum stress intensity factor.[5–9,13] The high-temperature fatigue results of some selected ceramics and ceramic matrix composites[14–19] suggest that the viscous intergranular glassy phase, a product of either the sintering process due to the addition of sintering additives or oxidation at high temperature, significantly influences crack propagation behaviour and fatigue life. In most cases, cyclic loading leads to lower crack growth rates at elevated temperatures than static loading with the same maximum stress intensity factor.[15,19–21] This is the reverse of what has been reported from room-temperature studies. This difference is attributed to the rate-dependent nature of viscous deformation of the grain boundary glassy phases at high temperatures.[14,15,18,19]

---

*To whom correspondence should be addressed.

†Nuclear Electric, Technology Division, Canal Road, Gravesend DA12 2RS, UK.

Assuming that the mechanisms of crack growth under static and cyclic loads are the same, the relative crack growth rates under cyclic and static loading can be predicted by an integration of the crack growth velocity.[19,21–24] The crack velocity, v, has the following power-law dependence on the applied stress intensity factor, K

$$v = AK^n \tag{1}$$

where A and n are constants for the material under a particular set of conditions and K is equal to

$$K(t) = \sigma(t) Y \sqrt{\pi a} \tag{2}$$

where $\sigma(t)$ is the time-dependent applied stress, Y is a geometric factor (which is dependent on normalized crack length in finite specimen geometries, but is often assumed to be effectively independent of crack length) and a is the crack length.

The ratio of the cyclic and static velocities, and therefore inverse times to failure, is approximately

$$\frac{v_c}{v_s} = \frac{t_s}{t_c} = \frac{\int_0^{1/f} \sigma_c^n(t)dt}{\sigma_c^n} \tag{3}$$

where f is the cyclic test frequency. For a static load equal to the peak cyclic load, this predicts that cyclic growth rates will be smaller than static rates. At room temperature the measured cyclic crack growth rates are in fact higher than the static fatigue rates. This indicates that a true mechanical fatigue effect exists and that cyclic fatigue is not simply a manifestation of static fatigue effects.[24] At high temperature the cyclic crack growth rates are lower than the static rates, but their ratios are not necessarily consistent with the ratios predicted above.[21] It is therefore obvious that different fatigue mechanisms must operate for the same ceramic material at different temperatures. The adhesive effect of viscous grain boundary phases on crack surfaces was proposed to explain the deviations between the predictions and measurements for the high-temperature fatigue of ceramics.[14] Cyclic fatigue behaviour and lifetime predictions are consequently even more complicated at high temperatures than at room temperature. Factors such as test frequency, cyclic waveform and creep, which may have little relevance at room temperature, become important at high temperatures.

The high-temperature fatigue life of silicon nitride has been investigated by several workers,[14,17,25,26] but there are only a few publications concerning high-temperature fatigue crack growth in silicon nitride or other ceramics.[19,21,27] In most of the reported investigations, the fatigue specimens were enclosed in a large, fully closed furnace and the tests were periodically interrupted for the crack length measurements. This involved lengthy periods for furnace cool-down and heat-up together with careful preparation of specimen surface replicas. It was justified that such interruptions did not affect the measured crack growth rates.[21]

In this study, a furnace arrangement was used that eliminated the need to interrupt the fatigue test and enabled the subcritical growth of long cracks (>100 μm) to be monitored continuously *in situ*.[28,29] Also, the fatigue crack growth behaviour of small surface flaws (>50 μm) was investigated by push–pull fatigue testing of machined cylindrical specimens. The fatigue crack growth behaviour of a silicon nitride at 1000°C is reported, and a possible crack growth mechanism is proposed in light of the fatigue test results and microscopic observations.

2 Materials and Experimental Techniques

The material studied was a gas-pressure-sintered silicon nitride (GPSSN) with yttra and alumina additives supplied by NGK Spark Plug Co., Japan. The as-received material consisted principally of β-Si_3N_4, which had an elongated grain structure with the aspect ratio of the grains varying from between 1 to 5. The grain diameter (measured across the basal plane) was up to 1·0 μm (Fig. 1). The porosity of the material was low (<1%). The silicon nitride grains were separated by a very thin, glassy, intergranular phase, which was found through high-resolution lattice imaging to be 1·0–2·0 nm thick between adjacent Si_3N_4 grains. This amorphous glassy phase, which was located mainly at multi-grain junctions, contained Y, Al, Si and O [Fig. 2(a)]. Most of the glassy phase crystallized at some grain boundaries during the high-temperature fatigue testing [Fig. 2(b)]. Similar crystallization behaviour was found in a

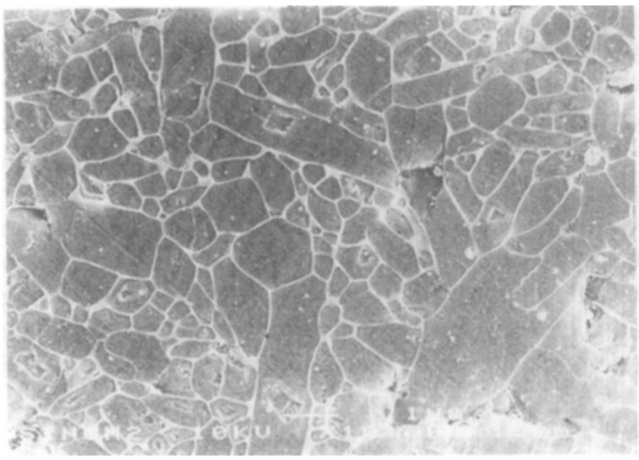

Fig. 1. Microstructure of as-received gas-pressure-sintered silicon nitride revealed by plasma etching.

similar silicon nitride after high-temperature annealing and creep testing.[30] The crystallization of the intergranular phase is likely to have a significant influence on high-temperature mechanical behaviour.

Double cantilever beam (DCB) specimens were used for the slow crack growth experiments [Fig. 3(a)]. These specimens were polished progressively using 14 μm, 6 μm, 3 μm and 1 μm diamond pastes on a lapping machine. They were subsequently cleaned ultrasonically in an acetone bath to reveal polished, shiny surfaces which were necessary for crack observation and length measurements during the high-temperature fatigue tests. A groove, 0·7 mm wide and 1 mm deep, was cut into the reverse side of the specimens in order to confine the growth of the fatigue crack through the centre of the specimen.

For the slow crack growth experiments a compact and accessible furnace was used in which the DCB specimens were heated directly by infra-red radiation.[28,29] This furnace allowed both cold gripping of the specimen and direct viewing of the growing crack. It was installed on a Mayes servo-hydraulic testing machine. The crack was monitored through air-cooled windows and its length measured with a travelling microscope which was mounted on a micrometer stage on the furnace casing. The furnace temperature was measured using a Pt/Pt–13Rh thermocouple placed at the base of the specimen notch.

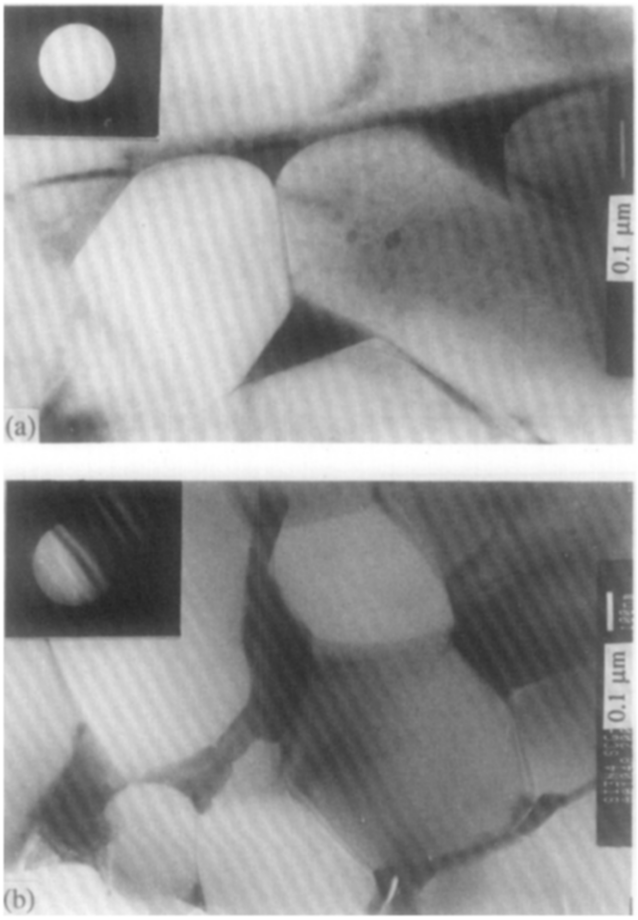

Fig. 2. Intergranular phases in silicon nitride and corresponding convergent beam electron diffraction patterns: (a) as-received material; and (b) material tested at 1000°C.

In the current investigation, the infra-red radiation from the heaters was de-focused to produce bands of heating near the specimen edges. A near constant temperature distribution (1010 ± 10°C) was obtained across the specimen in the area of interest [Fig. 4(a)]. The temperature gradient introduced thermal stresses in the specimen and these were calculated from the temperature distribution via a finite element method. The most important thermal stress components caused by the furnace set-up were the stresses normal to the direction of crack propagation. For a crack of 16·5 mm in length (a/w = 0·43), the normal stress was tensile within a distance of 3 mm ahead of the crack tip and was compressive over greater distances. This stress distribution translated with the tip of the crack as it propagated, so that the stress profile seen by the crack tip remained nearly constant. The magnitude of the stress intensity factor, K_t, produced by these normal thermal stresses was calculated and found to be of the order of 0·4 MPa $m^{1/2}$ for most crack lengths. In the calculations, it was assumed that the temperature distribution was not changed when the crack propagated. The value of K_t is taken into account in our calculation of the total stress intensity factor at the crack tip during the high-temperature fatigue test.

Because there are no published formula for the short DCB specimen geometry used in the current investigation, the compliance method was used to experimentally obtain the stress intensity factor K_I for a varying crack length. A steel specimen of the same geometry and size as the ceramic specimen was used and a capacitance displacement transducer was attached to the specimen to measure the notch opening displacement with a resolution of better than 0·1 μm. Figure 5 shows the experimentally determined calibration of the normalized stress intensity factor, $K_I B\sqrt{w}/P$, with crack length for the short DCB specimen (w/h = 3·0), together with published data for DCB specimens of different dimensions. B is the specimen thickness, w is the specimen length shown in Fig. 3(a) and P is the applied load.

The slow crack growth experiments were conducted using both static loading and cyclic sinusoidal loading at a frequency of 1 Hz. The specimen was pre-cracked at 1000°C prior to the beginning of the fatigue test by slowly applying a monotonic tensile load while the notch tip was being observed through the travelling microscope. As soon as a crack appeared at the notch tip, the load was reduced to zero. The pre-crack length obtained was then approximately 4 mm. The testing was started with an initial static load of 50 N which was increased in steps of 10 N every 30 min until crack propagation was observed. Each time the loading condition (static or cyclic) was changed, the test was re-started with a low load and the procedure described above was repeated. In between the different loading conditions, the testing was stopped, the load reduced to zero before the specimen was cooled and the specimen removed from the testing machine for examination of the crack path under a field-emission scanning electron microscope (JEOL 6300F). The specimen fractured catastrophically at the end of the final static fatigue test when no attempt was made to reduce the crack growth rate. The heaters were switched off instantly and compressed air jets forced rapid cooling of the fractured specimen.

The push–pull specimens were machined by rotary grinding with a diamond-bonded wheel (grit size 240) into double-waisted cylindrical specimens [Fig. 3(b)]. The specimens were machined to strict tolerances of both size and straightness to minimize bending stresses on loading. Some of the specimens were tested in this as-machined state and others were annealed at 1000°C in air for 27 h prior to testing; to distinguish between them they are referred to 'as-machined' and 'annealed', respectively. In the push–pull tests the specimens were heated using two parabolic radiant heaters, of 750 W power each, focused into spots of 6 mm diameter on the central gauge length. The ends of the specimens were friction clamped with water-cooled hydraulic grips with facilities for alignment and adjustment in tilt and shift. The specimen temperature was controlled to ±2°C with a thermocouple (Pt.Pt–13%Rh) looped around the centre of the gauge length. The temperature profile along the specimens is shown in Fig. 4(b), where it can be seen that there was a temperature drop of less than 100°C between the centre and end of the specimen gauge length. Of the 21 specimens tested, only four

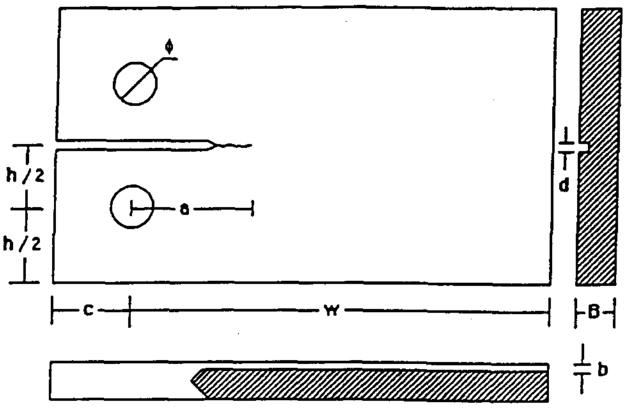

	h	ϕ	c	w	d	B	b
Dimension (mm)	12.50	4.50	7.56	38.00	0.70	4.00	1.00

(a)

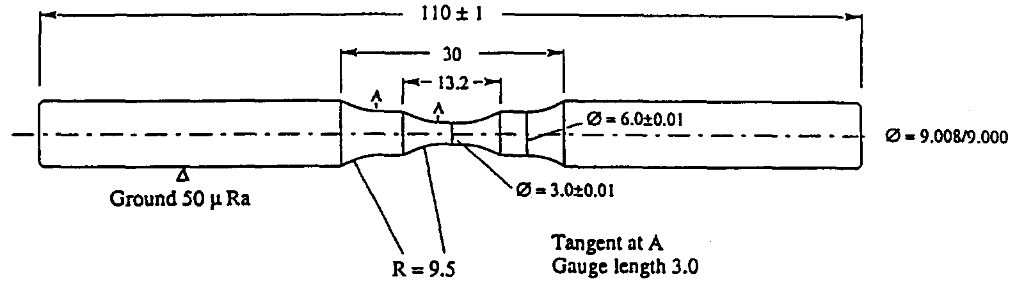

(b)

Fig. 3. Specimen geometries used for fatigue testing: (a) slow crack growth; and (b) push–pull.

did not fail at the very centre of the gauge length, and the results of these tests have not been used. For the other specimens, the regions where fatigue failure occurred corresponded therefore to the region with the maximum, nominal test temperature. The cyclic tests were performed at a frequency of 10 Hz, using fully reversed loading (R = −1, where the load ratio, R = minimum load/maximum load) and a sine waveform. The load amplitude was applied slowly by increasing from zero to the test amplitude at a rate of 10 MPa s^{-1}.

The scatter of push–pull fatigue data is strongly influenced by the inherent scatter of the strength of the ceramic. For this reason it is necessary to test many specimens in order to plot an *S–N* fatigue curve. The magnitude of this scatter is inversely related to the Weibull modulus, m, of the material. Additional scatter of the data is introduced by bending strain introduced by specimen misalignment. In fact, the most critical part of uniaxial push–pull testing is to achieve good alignment. This is difficult and time-consuming to achieve, and it is therefore necessary to determine some 'appropriate' level of alignment that needs to be achieved. If the scatter introduced by the inherent variability of the strength of the material is relatively large, small misalignments may have a negligible influence on the results. The Weibull cumulative probability of failure is defined as

$$P_f = 1 - \exp\left\{-\left[\frac{\sigma - \sigma_u}{\sigma_o}\right]^m \frac{V}{V_o}\right\} \qquad (4)$$

$$Ln(1 - P_f) = -\left[\frac{\sigma - \sigma_u}{\sigma_o}\right]^m \frac{V}{V_o}. \qquad (5)$$

The terms V_0 and σ_0 are normalizing volume and stress terms, respectively, and V is the specimen

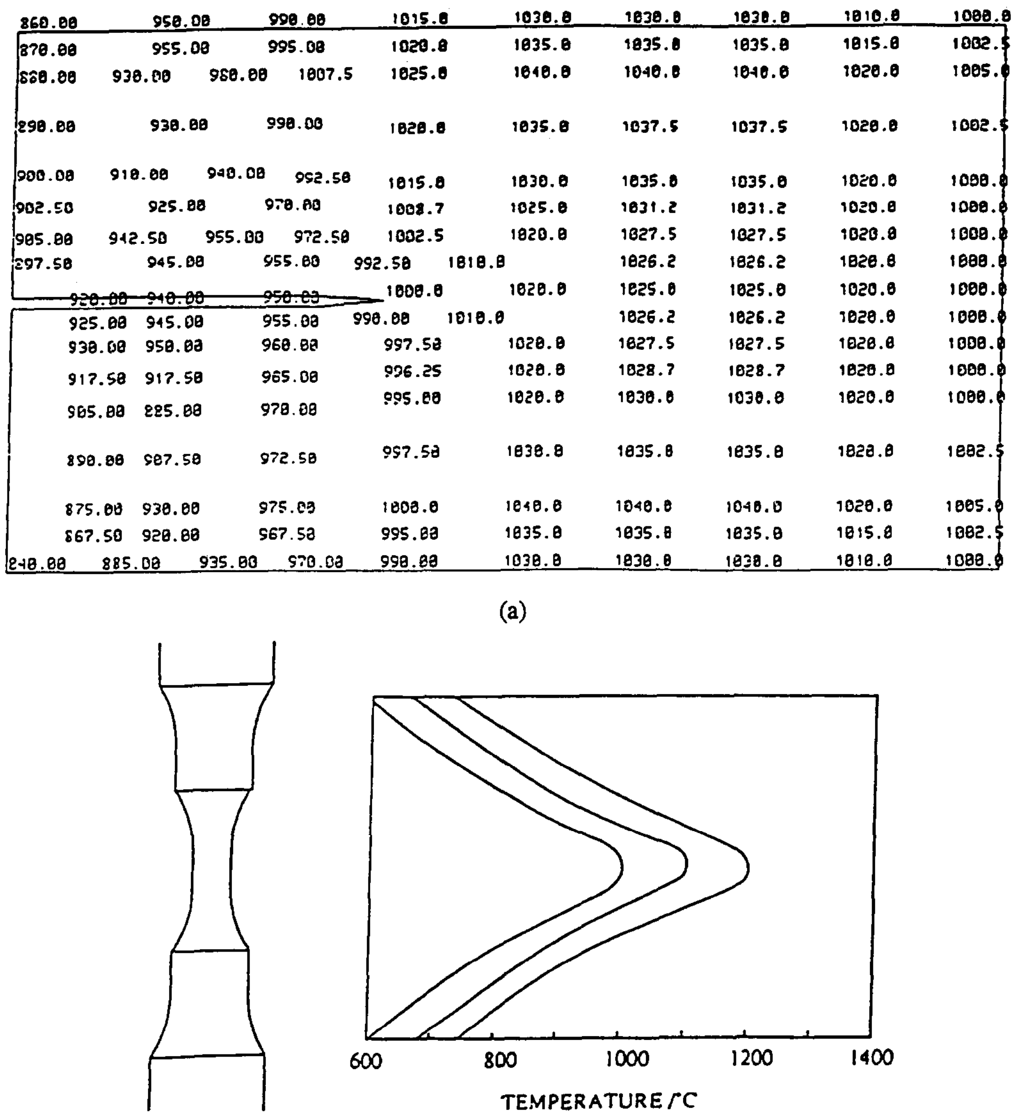

(a)

(b)

Fig. 4. Temperature distribution in fatigue specimens: (a) slow crack growth; and (b) push–pull.

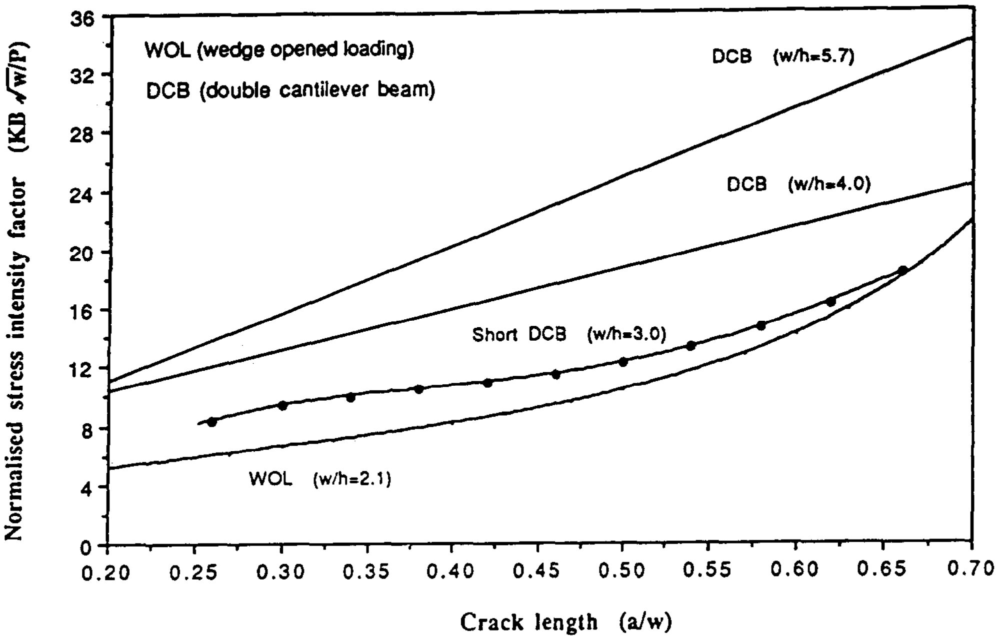

Fig. 5. Calibrated normalized stress intensity factor as function of crack length for slow crack growth specimen geometry.

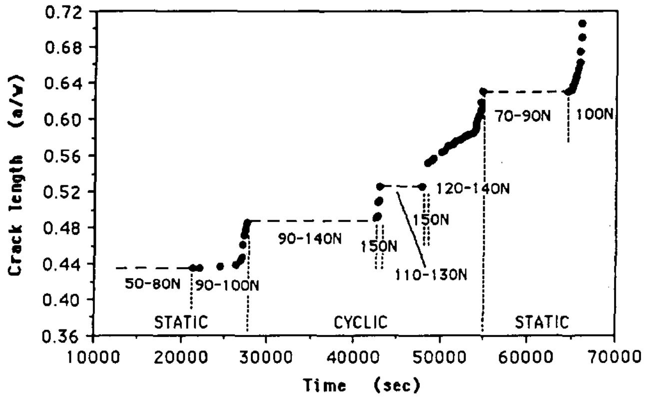

Fig. 6. Crack length as a function of time during static and cyclic slow crack growth experiments. Indicated are initial and final maximum applied loads for each loading sequence.

test volume, which is the same for identical specimens. The threshold stress, σ_u, is usually assumed to be zero, so that

$$Ln(1 - P_f) \propto - \sigma^m. \quad (6)$$

The ratio of the failure stresses corresponding to probabilities of failure of 0·95 and 0·05 is therefore

$$\frac{\sigma_{0.95}}{\sigma_{0.05}} = \left[\frac{Ln(1-0.95)}{Ln(1-0.05)}\right]^{1/m}. \quad (7)$$

If we arbitrarily say we will tolerate scatter produced by bending equivalent to 10% of this, the relative bending stress would be

$$\frac{\Delta\sigma}{\sigma} = 0.1\left(\frac{\sigma_{0.95}}{\sigma_{0.05}} - 1\right). \quad (8)$$

Assume $m = 10$ typically

$$\frac{\Delta\sigma}{\sigma} = 0.05 \quad (9)$$

and therefore the corresponding relative bending strain is

$$\frac{\Delta\varepsilon}{\varepsilon} = 0.05 = 5\%. \quad (10)$$

The alignment of the test machine was measured and corrected using a push–pull specimen with a triad arrangement of strain gauges. This enabled both the direction and magnitude of the relative bending strain to be determined. On initial loading the relative bending strain was usually >5%. With increasing stress the bending strain decreased exponentially, and extrapolated to the failure stresses, the relative bending strain at failure was always <5%.

3 Results

3.1 Mechanical experiments

The normalized crack length (a/w) as a function of test time for the different loading conditions for the slow crack growth experiments at 1000°C is shown in Fig. 6. Values in the figure indicate the applied constant tensile loads for static fatigue or the maximum applied loads for cyclic fatigue. When the maximum load was progressively increased the initial and final maximum loads are indicated. The crack started advancing at a static load of 90 N with a crack growth rate of approximately 2×10^{-8} m s^{-1} and accelerated at the constant load of 100 N. The static load was then reduced to 90 N to achieve stable crack propagation. The initial static fatigue test was stopped at the normalized crack length of a/w = 0·486. Subsequently, the loading condition was changed to cyclic loading with R = 0·3. The crack did not

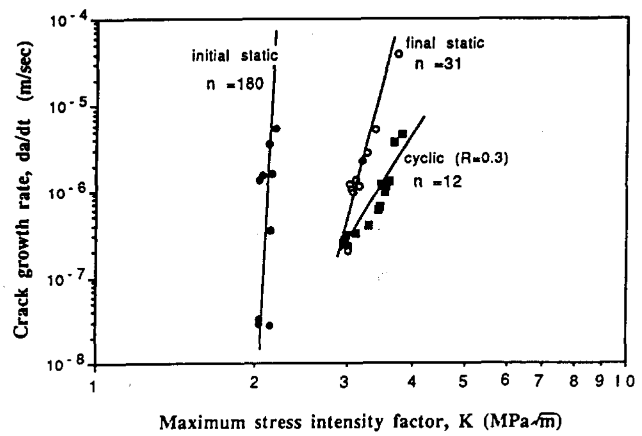

Fig. 7. Fatigue crack growth rates for static and cyclic fatigue at 1000°C and $R = 0{\cdot}3$ (data corrected for thermal stress intensity factor).

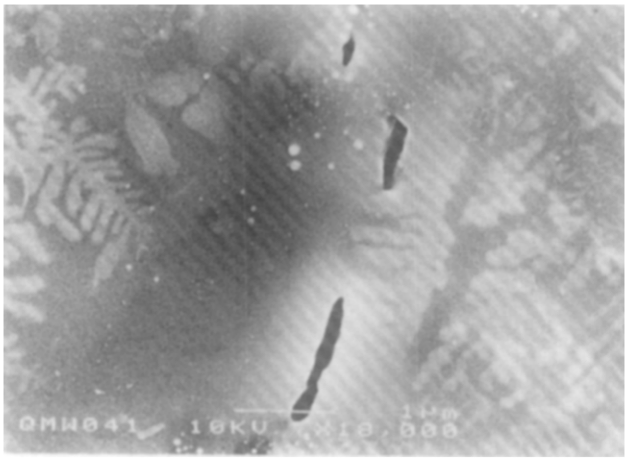

Fig. 8. Crack path profile. Note residual opening, rounded appearance of oxidized grain surfaces and mismatch of crack faces.

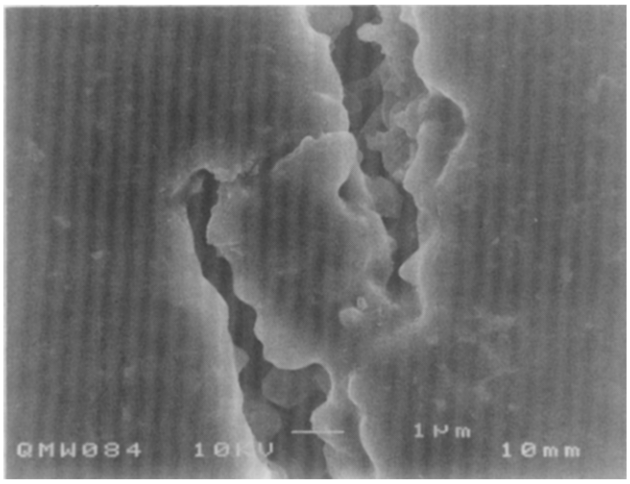

Fig. 9. SEM micrograph of fatigue fracture path at 1000°C in slow crack growth specimen, showing creep cavities ahead of statically grown crack.

propagate until the maximum load was increased to 150 N. A series of static and cyclic tests was then performed (Fig. 6) until the specimen eventually fractured.

Using the data of Fig. 6, the crack growth rates were determined from the gradients of the curves. The corresponding stress intensity factors were determined using the data for the DCB specimen geometry (see $w/h = 3{\cdot}0$ in Fig. 5). Figure 7 shows the logarithmic crack growth rate plotted as a function of the logarithmic maximum stress intensity factor. The data have been corrected to account for the stress intensity factor K_t produced by the thermal gradients in the specimen. The crack growth rate can be reasonably well fitted to a power-law relationship like eqn (1).

The exponent n is larger for static fatigue than for cyclic fatigue. Similar results have been reported for other ceramics where the stress intensity factor range, ΔK, was found to characterize the crack growth rates.[21] The crack propagated faster under static loading than under cyclic loading with the same maximum stress intensity factor. This observation is consistent with the results reported for other ceramics,[15,19] and is also consistent with the longer lifetime obtained for silicon nitride under cyclic loading at high temperatures.[14,17,25,26] The fatigue behaviour at elevated temperatures is contrary to what is found at room temperature, where cyclic loading has a more deleterious effect on resistance to fatigue fracture than static loading.[11,13] These results are also in agreement with a previous observation by others that the GPSSN studied is highly fatigue-resistant up to 900°C but becomes susceptible to cyclic and static slow crack growth at 1000°C.[26] The large differences in the sets of data for the initial and final static fatigue tests may be attributed to increasing crack growth resistance with increasing crack length.

The crack paths and profiles were examined by scanning electron microscopy (SEM) on the surface of the specimen after the different loading conditions. The crack always had a large residual opening over its entire length and it was easy to look into its wake. The grain and fracture facets were rounded and their shape obliterated by a solidified amorphous layer (Fig. 8). Hence the fracture surfaces were heavily mismatched and this must have been largely responsible for the residual opening of the crack. Rounded large cavities could be seen ahead of the crack tip after the initial static fatigue test (Fig. 9). This cavitation may have been a surface effect not characteristic of the bulk behaviour since we believe it was associated with the presence of a viscous glass layer formed by the relatively heavy oxidation of the specimen surface. Evidence of this oxidized surface is provided by the dendritic growth of a crystalline phase in the oxide (Fig. 9) and by observations of the fracture surfaces, as discussed later. No large differences existed between the crack profiles of

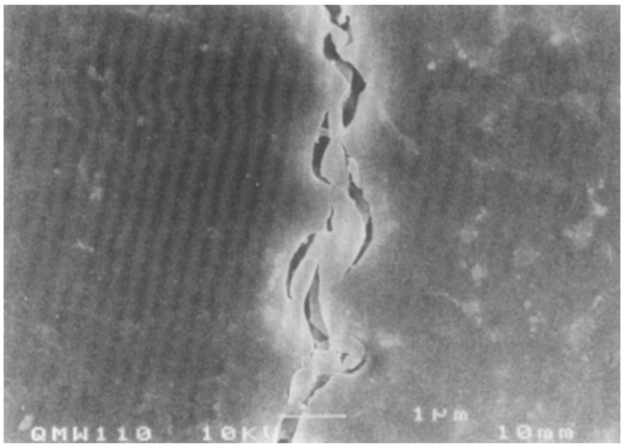

Fig. 10. Secondary cracking and the formation of crack wedges during cyclic loading.

cracks grown statically and cracks grown under cyclic loading, except that more secondary cracks appeared in the latter. With an increasing number of cycles some of the secondary cracks (which always appeared open) propagated and linked with the main crack, forming wedges between the crack faces (Fig. 10).

On the fracture surfaces of broken specimens the regions of slow crack growth and the regions of fast fracture were clearly distinguishable. The slow crack growth regions were covered with an amorphous layer of solidified glass that was produced by oxidation. Near the crack mouth (notch end), where the surfaces were exposed to air for a longer time, the grain texture was completely destroyed [Fig. 11(a)]. Nearer the tip of the crack, where the oxidation was less severe, some granular texture remained [Fig 11(b)]. All around the edges of the fracture surface a 10-μm-thick oxidized surface layer was apparent (Fig. 12). This process of oxidation must have played an important part in the slow growth of the crack.

The cyclic push–pull fatigue data are shown in Fig. 13(a). The strength of the as-machined and annealed specimens, extrapolated to a fracture time of 10 s, is ~500 MPa and 700 MPa, respectively. The annealed specimens are therefore approximately 40% stronger than the as-machined specimens. The difference was such that the annealed specimens did not fail after 10^6 cycles under cyclic loading, whereas these conditions caused fatigue fracture of the as-machined specimens. This increase in strength and fatigue resistance could have been a consequence of flaw healing during the annealing treatment and this possibility is examined later. The cyclic fatigue data for the annealed specimens are compared with static fatigue data for annealed specimens in Fig. 13(b). Consistent with the v–K data in Fig. 7(b), static loading is considerably more damaging than cyclic loading.

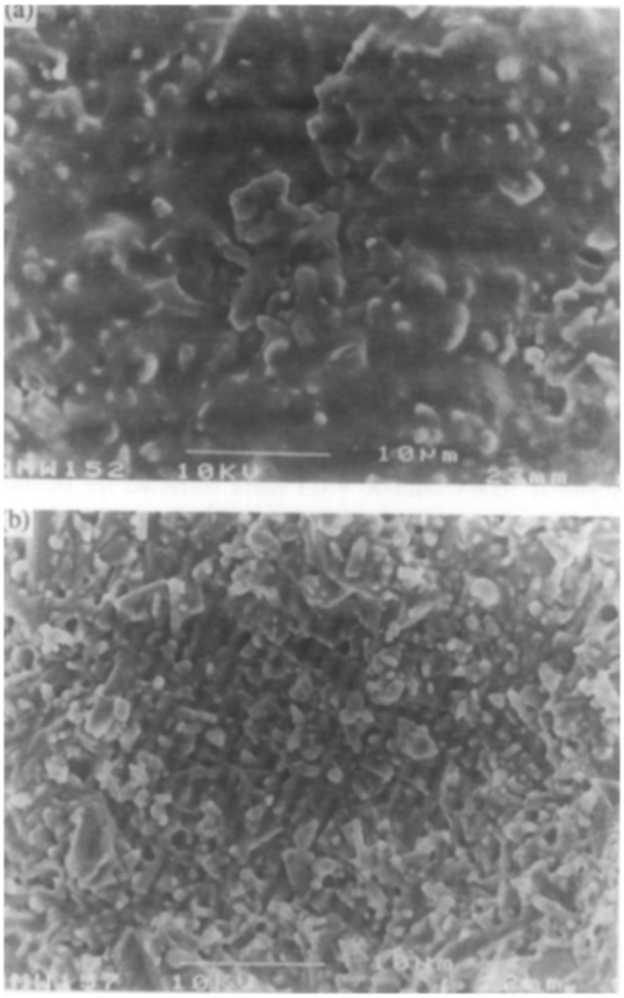

Fig. 11. Fracture surfaces: (a) near crack notch; (b) nearer crack tip just prior to fast fracture.

Assuming crack growth was controlled by static fatigue effects during cyclic loading, the relative times to failure under static and cyclic loading can be calculated using eqn (3). Using a value of n = 60, this gives the ratio of times to failure tc/t_S = 19·5. The broken line in Fig. 13(b) shows the position of the predicted static data based on the cyclic data, and there is clearly no correlation with the experimentally determined static data.

The stress exponents n, determined from the push–pull testing are 16 and 60 for static and cyclic fatigue, respectively. Accepting that the intrinsic scatter of the data is large, there is no correlation of these values and those generated by the v–K curves from the slow crack growth experiments (Fig. 7). The reason for this is not clear, and may be a consequence of the large differences in the crack length in the two types of test, implying that n has little meaning as a fatigue parameter.

Microscopical observation of the specimens fractured under both static tensile load and push–pull revealed a dark band with a thickness of between 10 and 70 μm, which corresponded to an oxidation layer [Figs 14(a) and (b)]. This surface

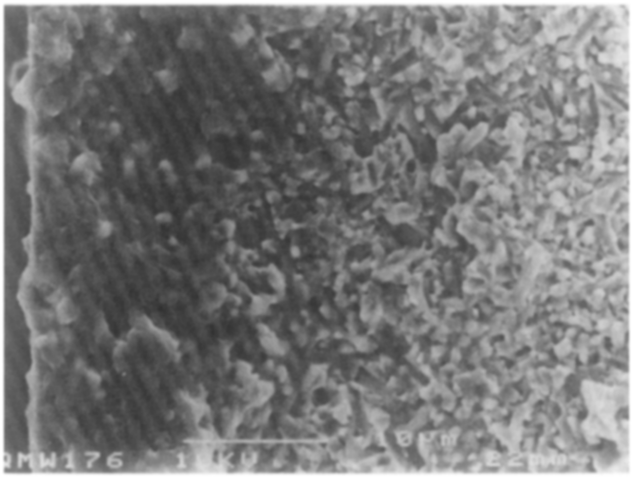

Fig. 12. Oxidized surface layer (~10-μm-thick) at the edge of a tested slow crack growth specimen.

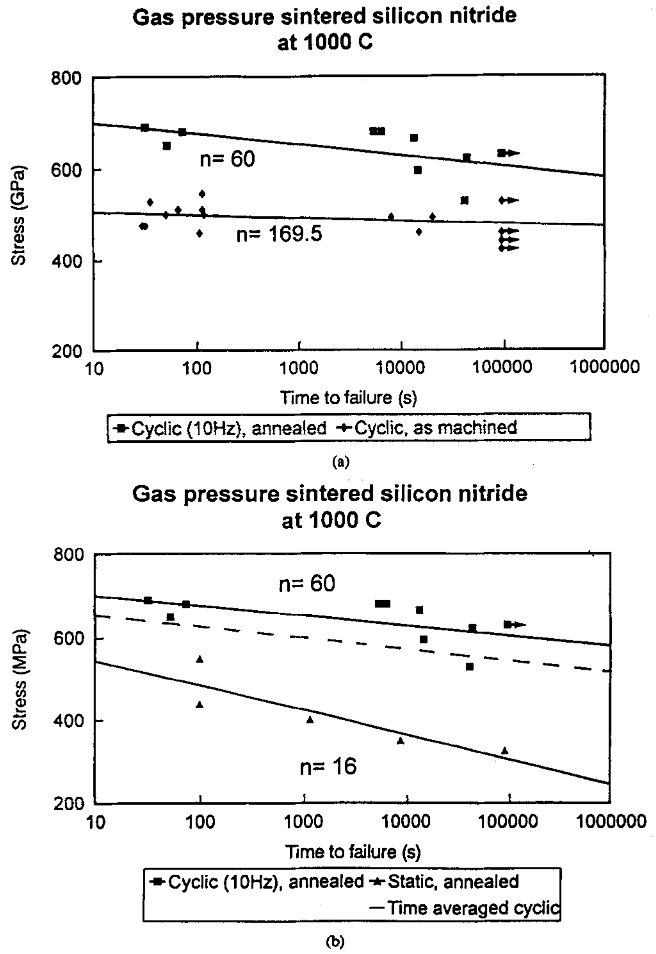

Fig. 13. Static and cyclic push–pull fatigue data at 1000°C and $R = -1$: (a) comparison of cyclic data for as-received and annealed specimens; and (b) comparison of cyclic and static data. Broken line represents time-averaged predicted static fatigue data based on the cyclic data.

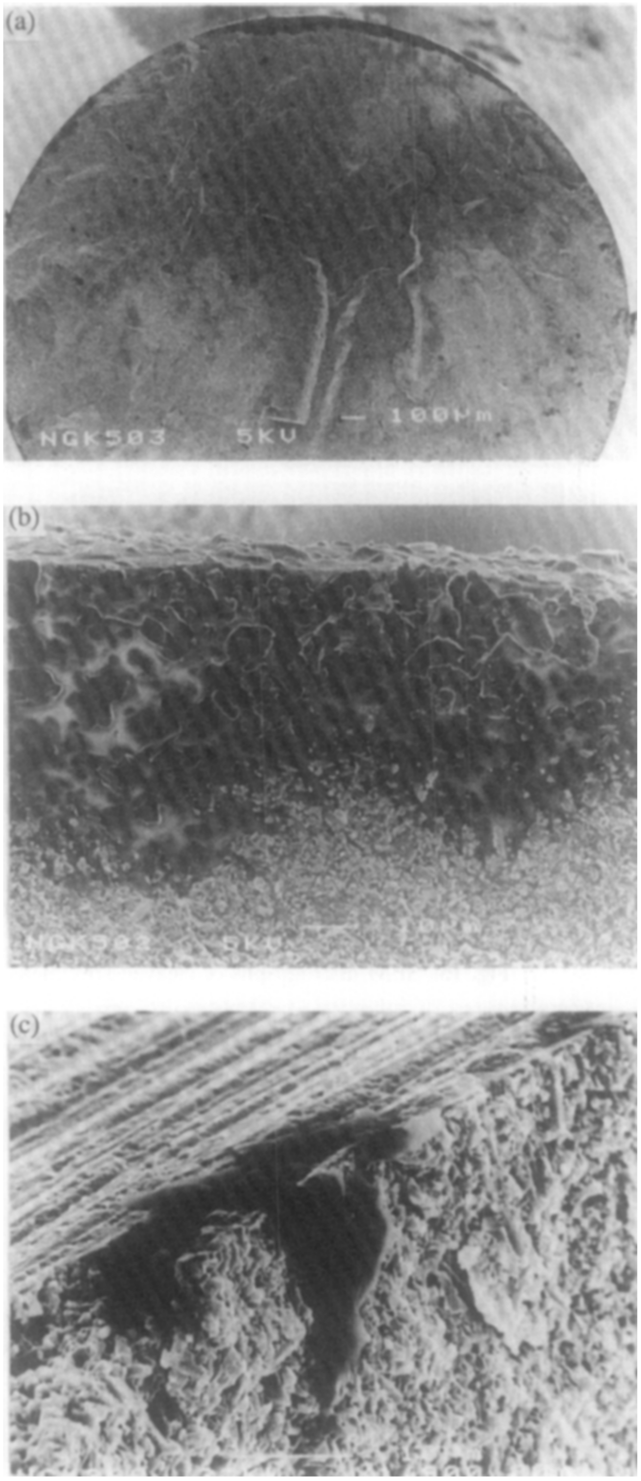

Fig. 14. Fracture surface of push–pull specimen fatigue tested at 1000°C: (a) dark band around the edge of specimen was produced by oxidation, and the widest region of the band (~70 μm) corresponds to fracture origin; (b) high magnification image of edge of fracture surface; and (c) extruded debris at edge of specimen.

oxide layer was, not surprisingly, similar to that observed on the surface of the slow crack growth specimens. The low-magnification fractography of these specimens clearly showed the regions of crack initiation, slow crack growth and fracture. The region where the oxidation layer was thickest corresponded to the crack initiation region. At places around the surfaces of the tested push–pull specimens, tongues of extruded material could be seen [Fig. 14(c)]. These gave the impression of being the oxide glass having been exuded from the cracks during the compressive loading.

3.2 Oxidation experiments

In order to study in a controlled manner the formation of the oxide glass phase on the exposed surfaces of the specimens at 1000°C, some small

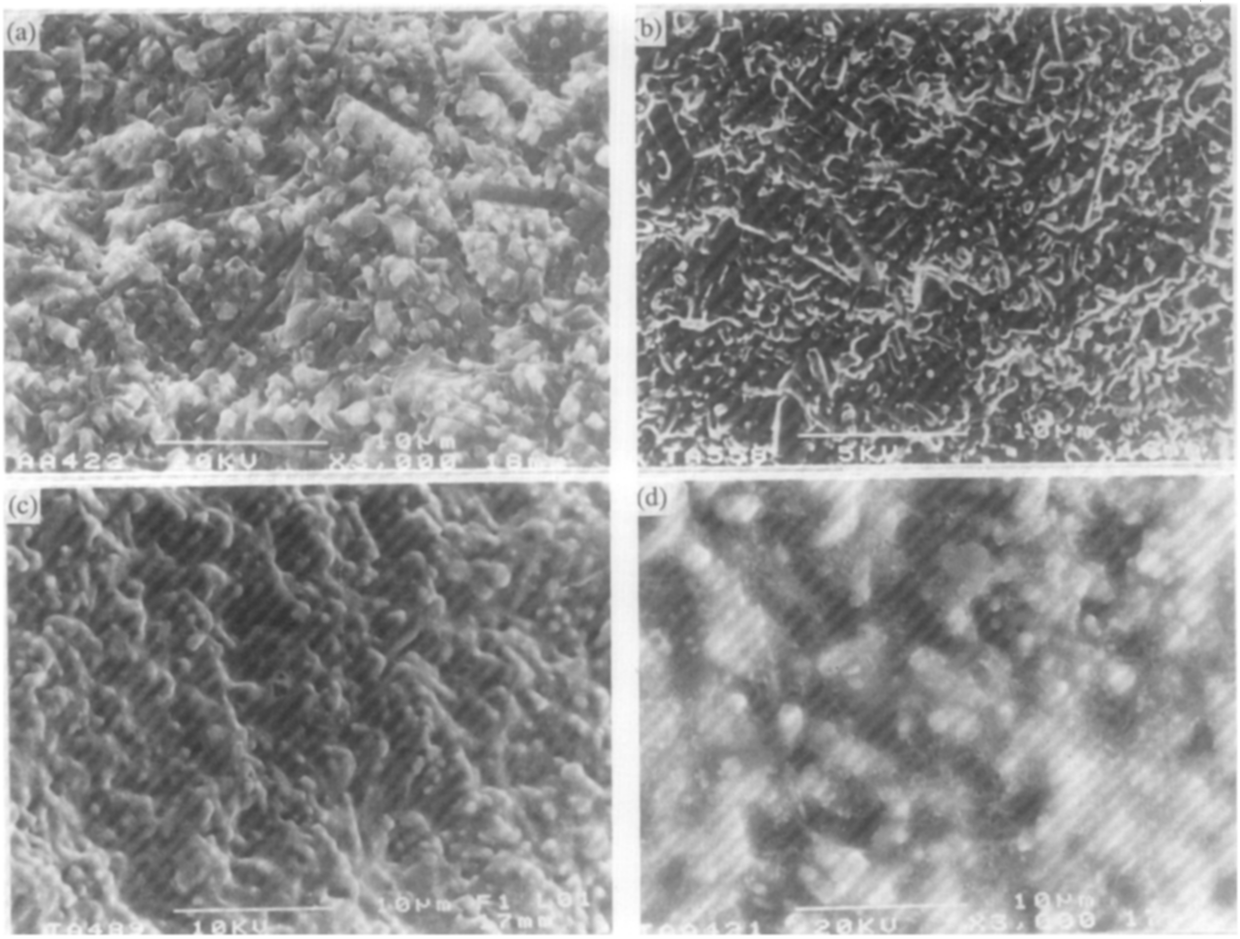

Fig. 15. SEM micrographs of cleaved specimens oxidized at: (a) 850; (b) 900 (c) 950; and (d) 1000°C.

samples with freshly cleaved surfaces and some with polished surfaces were annealed in air for 27 h at temperatures of 850, 900, 950 and 1000°C. The oxidized cleaved surfaces had exactly the same appearance as those of the oxidized fractured specimens. Heat treatment above 950°C produced a thin layer of glassy phase within which a needle-like crystalline phase had precipitated (Fig. 15). Examination by transmission electron microscopy (TEM) and energy-dispersive spectroscopy analysis of the oxidized surfaces confirmed that the needle-like phase was an yttrium silicate containing Al and Ca. The glass layer was silica formed by the oxidation of the silicon nitride. This oxidation is very rapid on an uncontaminated, freshly cleaved surface and it was accompanied by the diffusion of the cation additives (Y^{3+} and Al^{3+} and impurities, Ca^{2+}) from the grain boundaries. Small concentrations of the low melting point elements dramatically reduce the viscosity of the glass which evidently could flow very easily at 1000°C and washed-out the granular texture of the fracture surfaces. No significant oxidation of the material was detected after heating for 27 h below 950°C (Fig. 15). TEM observations also revealed numerous voids in the intergranular regions close to the oxidized surface in specimens annealed at 1000°C (Fig. 16).

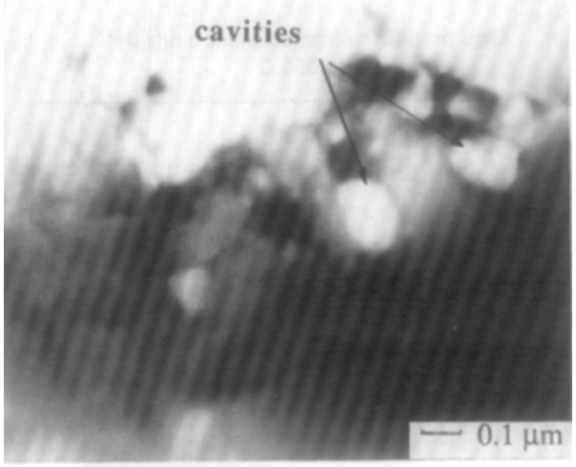

Fig. 16. TEM micrograph at interface between silicon nitride and surface oxide layer produced at 1000°C. Cavities are apparent at some grain boundaries.

The possibility of crack healing at high temperature was investigated by annealing experiments with indentation-produced flaws [Fig. 7(a)]. After annealing at 1000°C for 3 h the radial surface cracks were no longer clearly apparent and appeared to be welded together at some local regions by an amorphous phase [Fig. 17(b)]. This is confirmation that it is possible that surface machining flaws can be healed locally by what appears to be a glassy phase (produced by oxida-

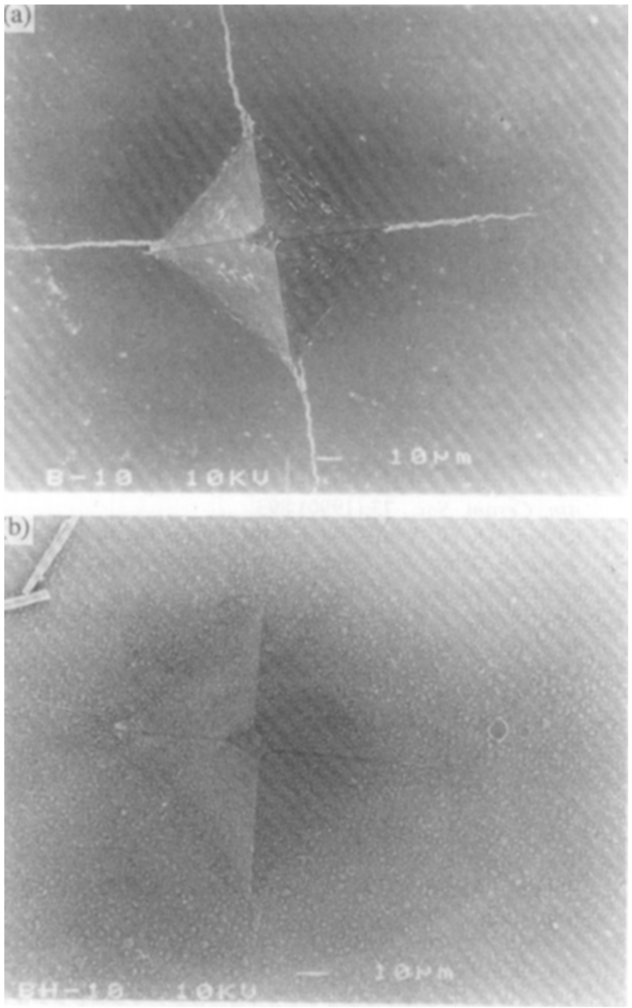

Fig. 17. Vickers indentation impression: (a) before; and (b) after annealing for 3 h at 1000°C.

tion) which can flow easily at the temperature of the tests. The closure of the crack also indicates that the plastic zone at the indentation impression, which produces the residual stress that opens the radial cracks, must have been relaxed by annealing.

4 Discussion

The results of the present investigation have revealed the importance of oxidation in the process of slow crack growth in Si_3N_4 at 1000°C in air. Our observations are consistent with the findings of others that isostatically pressed Si_3N_4 was not susceptible to subcritical crack growth in an inert environment at 1370°C, whereas the same material tested in air showed a strong fatigue susceptibility.[31] Other work[26] on the same material used in our study showed that, up to 900°C, the material has similar crack propagation properties and strength as at room temperature, while these properties are considerably degraded at 1000°C, coincident with the temperature at which oxidation becomes significant. All these observations suggest that the low-temperature crack growth mechanism changes at 1000°C when oxidation takes place and a relatively low viscosity phase is formed. In these oxidizing conditions, a crack, or pre-existing flaw, can grow by the co-operative effect of stress, oxidation and flow of the glass phase. The effect of stress, by forcing the crack open, is that of assisting the oxygen transport to the crack tip where an oxidized zone (not necessarily very deep) is formed and the crack can eventually advance by the flow of the low viscosity oxide phase. The rate of growth of the crack is determined in a complex manner by the applied stress, rate of oxidation, the rate at which Al^{3+} and Ca^{2+} can diffuse from the grain boundaries to the oxide layer and by the rate of flow of the glass. It is therefore not surprising to find that the relationship between crack velocity and applied stress intensity factor is different for different specimen geometries and different crack lengths, since geometrical factors can influence the rates of oxide formation at the tip of cracks and the rate of its viscous flow. It is noted, for example, that the average subcritical velocities in the tensile and push–pull specimens ($\sim 5 \times 10^{-9}$ m s^{-1}) were considerably slower than those measured in the slow crack growth experiments. The surface cracks in the former are very short (20–100 μm) and their faces are more effectively welded together by the glass phase. This could explain the flaw healing effect of the annealing heat treatment at 1000°C and the strength increase of the annealed specimens. Both the slower growth of cracks, and longer fatigue life of specimens under cyclic fatigue have also been observed by others in Si_3N_4 and Al_2O_3 at high temperatures.[14,15,17–20,26] This behaviour points to the absence of genuine cyclic fatigue effects at high temperature, and that periods of crack opening are more damaging than crack cycling.

The oxidized fracture surface regions, observed by other workers and described by them as degradation zones,[31] act as markers for the crack geometry. On the tensile and push–pull specimens these markers revealed that the fracture origins were associated with surface cracks with a maximum depth of $a \approx 70$ μm. This information can be used to estimate fracture toughness using the expression $K = Y\sigma\sqrt{\pi a}$, where for half-penny cracks on a cylindrical rod, $Y = 0{\cdot}7$, and σ is the maximum tensile stress.[32] The critical value of K thus obtained is about 5·7 MPa $m^{1/2}$. This is similar to the values typically quoted for the fracture toughness, K_{IC}, of Si_3N_4 at room temperature determined using the indentation fracture toughness method. It should be noted that K_{IC} is relatively insensitive to temperature up to 1200°C,[33] as it should be if the toughness is determined by the onset of fast, unstable, crack propagation into the bulk material in the absence of oxidation effects. In the slow crack growth experiments, a well defined boundary between oxidation and fast fracture was not seen because the crack accelerates continually towards its critical length. Since crack length readings were taken at intervals, the true crack length at instability could not be determined from these tests.

5 Conclusions

1. (1) An experimental method has been developed that enables direct observation of the growth of subcritical fatigue cracks at high temperatures.
2. (2) The stress exponents, n, determined from high-temperature push–pull fatigue testing and slow crack growth experiments are inconsistent, indicating that n has little physical significance and is geometry-dependent.
3. (3) Annealing at 1000°C increases the strength of GPSSN by 40% as a consequence of oxidation-assisted crack healing and relaxation of surface-machining-induced residual stresses.
4. (4) The crack advancement mechanism at high temperature is influenced by oxidation at the crack-tip region and the formation of a viscous glassy phase. Oxidation ahead of the crack tip produces voids at the intergranular boundary. The stresses at the tip region of a tensile-loaded crack tend to increase the size and number of these voids by viscous flow. The coalescence of the voids produces a mechanism by which crack growth can occur. This mechanism explains the change in crack growth behaviour at high temperatures compared with room temperature.

Acknowledgements

We would like to thank NGK Spark Plug Co., Japan for supplying the GPSSN material. We also gratefully acknowledge the support of the SERC (now EPSRC), UK (GR/E 75844).

References

1. Ziegler, G., Heinrich, J. & Wotting, G., *J. Mater. Sci.*, **22** (1987) 3041.
2. Buljan, S. T. & Baldoni, J. G., in *Preparation and properties of Silicon Nitride Based Materials*, eds D. A. Bonnell & T. Y. Tien. Trans Tech Publications, Switzerland, 1989, p. 249.
3. Tressler, R. E., in *Ceramic Transactions, Vol. 10*, eds R. E. Tressler & M. McNallan. American Ceramic Society, Westerville, OH, 1990, p. 99.
4. Guiu, F., *Mater. Sci.*, **13** (1978) 1357.
5. Ewart, L. & Suresh, S., *J. Mater. Sci.*, **22** (1987) 1173.
6. Reece, M. J., Guiu, F., & Sammur M. F., *J. Am. Ceram. Soc.*, **72** (1989) 348.
7. Horibe, S., *J. Eur. Ceram. Soc.*, **6** (1990) 89.
8. Dauskardt, R., H., Marshall, D. B. & Ritchie, R. O., *J. Am. Ceram. Soc.*, **73** (1990) 893.
9. Kishimoto, H., Ueno, A. & Kawamoto, H., in *Fatigue of Advance Materials*, Proc. Engineering Foundation Int. Conf. CA, USA, 1991, p. 255.
10. Ritchie, R. O. & Dauskardt, R. H., *J. Ceram. Soc. Jpn*, **99** (1991) 1047.
11. Guiu, F., Li, M. & Reece, M. J., *J. Am. Ceram. Soc.*, **75** (1992) 2976.
12. Dauskardt, R. H., *Acta Metall. Mater.*, **41** (1993) 2765.
13. Li, M. & Guiu, F., *Acta Metall. Mater.*, **43** (1995) 1859.
14. Fett, T., Himsolt, G., & Munz, D., *Adv. Ceram. Mater.*, **1** (1986) 179.
15. Han, L. X. & Suresh, S., *J. Am. Ceram. Soc.*, **72** (1989) 1233.
16. Suresh, S., in *Fracture 90, Vol. 2*, eds H. Kitagawa & T. Tanaka. Materials and Component Engineering Publications Ltd, Birmingham, UK, 1990, p. 759.
17. Masuda, M., Soma, T. & Matsui, M., *J. Eur. Ceram. Soc.*, **6** (1990) 253.
18. Lin, C. K. J. & Socie, D. F., *J. Am. Ceram. Soc.*, **74** (1991) 1511.
19. Ewart, L. & Suresh, S., *J. Mater. Sci.*, **27** (1992) 5181.
20. Liu, S.-Y, Chen, I.-W. & Tien T.-Y., *J. Am. Ceram. Soc.*, **77** (1994) 137.
21. Ramamurty, U., Hansson, T. & Suresh, S., *J. Am. Ceram. Soc.*, **77** (1994) 2985.
22. Evans, A. G. & Fuller, E. R., *Metall. Trans.*, **5A** (1974) 27.
23. Evans, A. G., Russell, L. R. & Richerson, D. W., *Metall. Trans.*, **6A** (1975) 707.
24. Evans, A. G., *Int. J. Fract.*, **16** (1980) 485.
25. Lin, C. K., Jenkins, M. G. & Ferber, M. K., *J. Mater. Sci.*, **29** (1994) 3517.
26. Talima, Y., Urashima, K., Watanabe, M. & Matsuo, Y., *Ceram. Mater. Comp. Engines*, (1989) 719.
27. Evans, A. G. & Wiederhozn, *J. Mater. Sci.*, **9** (1974) 270.
28. *UK Patent Application No. 9219221.0.*
29. Bushby, A. J., Guiu, F. & Sammur, M. F. R., in *Ultra Temperature Mechanical Testing*, eds R. D. Lohr & M. Steen. Woodhead Publishing Ltd, Cambridge, UK, 1995, p. 214.
30. Chadwick, M. M. & Wilkinson, D. S., *J. Am. Ceram. Soc.*, **76** (1993) 376.
31. Wereszczak, A. A., Breder, K. & Ferber, M. K., *J. Am. Ceram. Soc.*, **76** (1993) 2919.
32. Astiz, M. A., *Int. J. Fract.*, **31** (1986) 105.
33. Mizuno, M. & Okuda, H., *J. Am. Ceram. Soc.*, **78** (1995) 1793.